JOURNAL OF THERMOPHYSICS AND HEAT TRANSFER
Vol. 19, No. 1, January–March 2005

Numerical Investigation of High Reynolds Number Flows over Square and Circular Cylinders

S.-C. Lo,* K. A. Hoffmann,‡ and J.-F. Dietiker†
Wichita State University, Wichita, Kansas 67260-0044

Numerical solutions of flows at high Reynolds numbers are investigated by detached-eddy simulation (DES). Two cylinders in crossflow are selected as the test cases; flow around a circular cylinder is simulated at Reynolds numbers of 1.4×10^5 and 3.6×10^6 and simulation for a square cylinder is performed at a Reynolds number of 2.2×10^4. These simple geometries produce complex flow phenomena such as recirculation, vortex shedding, and unsteady turbulent separation, which are very common flows associated with complex geometries. However, most numerical simulations have been performed at low Reynolds numbers, and only a few are reported at high Reynolds numbers ranges. DES with the Spalart–Allmaras turbulence model is used for turbulent treatment. It functions as a Reynolds averaged approach in the near-wall region and transfers to large eddy simulation (LES) far from the wall. This procedure requires fewer grid points compared to LES. To assess the quality of solutions, the results are evaluated by comparison with experimental data and other numerical results. In addition, laminar solutions and trip functions are also investigated in the circular cylinder cases. Even though fewer grid points are used, most of the results compare well with experimental data and other numerical solutions.

Nomenclature

C_D	=	drag coefficient
C_{DES}	=	detached-eddy simulation (DES) turbulent model constant
C_p	=	pressure coefficient
C_{pb}	=	backpressure coefficient
C_s	=	Smagorinsky coefficient
D	=	circular cylinder diameter/side of square cylinder
d_w	=	wall distance of Spalart–Allmaras turbulence model
$\tilde{d}$	=	modified wall distance of DES model
f	=	lift shedding frequency
L_r	=	recirculation length
Re	=	Reynolds number
S	=	magnitude of the vorticity
Sr	=	Strouhal number
t	=	time
U_∞	=	freestream velocity
x, y, z	=	Cartesian coordinates
y^+	=	reduced coordinate
Δ	=	grid space
Δ	=	difference operator
θ	=	angle measured from stagnation point
θ_{sep}	=	separation angle
ν_t	=	kinematic eddy viscosity

I. Introduction

BECAUSE of the increase in computer power in the past 20 years, computational fluid dynamics (CFD) has emerged as an efficient and cost effective approach for prediction of complex flowfields. It is possible to predict flowfields in regions where it may be difficult or impossible to measure flow properties by experimental methods. However, there remain some difficulties with the application of CFD. Namely, the solution may be sensitive to the grid, numerical approach employed, damping terms used, etc. It is often necessary to perform systematic tests to obtain a convergent and accurate solution. This is because the solution depends on several factors, and sometimes it is challenging to improve the solution. There are several test cases for CFD, such as flat plate, compression corner, axisymmetric base flow, and blunt body to name a few. The flow past a cylinder is one of the most challenging and complex flowfields, even though the geometry is simple. The flowfield includes large three-dimensional, geometry-dependent vortex flow in the wake region, boundary-layer separation, recirculation bubble, transition, Reynolds number dependency, and turbulence. These flow phenomena are very common in most applications, such as aircraft at high angle of attack, flow past the landing gear, etc. Therefore, it is beneficial to understand these complex flow phenomena by simulating these simple geometries and investigating the accuracy of solutions before extending the solution to more complex geometries. Furthermore, there are several experimental results over wide range of Reynolds numbers for the geometries considered, which provide the necessary data with which to compare the CFD results.

Grid generation is the first step for CFD calculations. An unstructured grid can be used to generate a grid for complex geometries or cluster cells in certain regions of interest. In addition, it also has the benefit of good scalability in parallel and ease of adaptation. However, the disadvantage of the unstructured grid is the difficulty in developing higher-order algorithms, and therefore, it is typically limited to second-order spatial accuracy. Furthermore, the memory requirement is higher than for the structured grid. In spite of these drawbacks, unstructured grids have been used successfully on many applications.[1–4]

Reynolds averaged Navier–Stokes (RANS) equations have been widely used in prediction of turbulent flows. They use turbulence models to simulate turbulent motion in the entire flowfield and are often adequate for steady flows and attached boundary layers. However, when the flowfield includes unsteadiness and massive flow separation, RANS is often unable to predict the flowfield accurately. One way to cross this barrier is to rely on large-eddy simulation (LES). However, the number of grid points required for accurate LES of a turbulent boundary-layer scales as $N \sim Re^2$ (Ref. 5), which becomes rather large for high Reynolds number flows. To overcome the deficiencies of RANS model for predicting massively separated flows, and reduce the computational load of the LES, Spalart et al.,[6] in 1997, proposed detached-eddy simulation (DES)

Received 16 March 2004; revision received 19 July 2004; accepted for publication 2 July 2004.

*Graduate Research Assistant, Department of Aerospace Engineering. Student Member AIAA.

‡Professor, Department of Aerospace Engineering. Associate Fellow AIAA.

†Visiting Assistant Professor, Department of Aerospace Engineering. Member AIAA.

using the Spalart–Allmaras (S-A) turbulence model[7] with the goal of developing a numerically feasible and accurate approach combining the most favorable elements of RANS and LES. In this approach, the attached boundary-layer turbulence would be modeled by RANS, whereas the larger detached eddies (populating the separation regions and wakes) would be simulated by LES. (Small eddies in this region are also modeled, but have less influence than boundary-layer eddies have.[8])

The effect of the Reynolds number on the boundary layer on the circular cylinder can be classified into three categories. When the Reynolds number is below 2×10^5, it is called the subcritical range. At this range of Reynolds numbers, the attached boundary layer is laminar, the separated shear layers are in the early stages of transition, and the wake is fully turbulent. When the Reynolds number reaches above 3.5×10^6, it is called the supercritical region, where the boundary layer starts as laminar, then transitions to turbulent before the separation takes place. The Reynolds number range from 2×10^5 to 3.5×10^6 is called the critical range. Based on drag coefficient distribution, Roshko[9] subdivided this region into lower transition ($Re = 2.5 \times 10^5 \sim 5 \times 10^5$) and upper transition ($Re = 1 \times 10^6 \sim 3.5 \times 10^6$) regions. In this range, the boundary layer begins as laminar and subsequently separates with turbulent reattachment, separation bubble, and finally turbulent boundary-layer separation. Achenbach[10] showed that the turbulent separation point for $Re = 8.5 \times 10^5$ can be up to 147 deg. Most numerical simulations are performed at low subcritical Reynolds number range because at this range the attached boundary layer is laminar and sufficiently thick to be easily resolved by computational grid, and therefore, the subgrid-scale (SGS) stresses of LES are relatively low. In the high subcritical or supercritical Reynolds number, the attached turbulent boundary layer becomes much thinner than in the low Reynolds number cases, for example, about six times thinner for $Re = 1.4 \times 10^5$ than $Re = 3.9 \times 10^3$. Because of the small boundary-layer thickness, the turbulent boundary layer simulation by LES becomes challenging inasmuch as it requires the grid to be sufficiently fine to resolve eddies at least as small as the boundary-layer thickness. In other words, the computer power requirement is much higher than for low Reynolds number cases. This is why there are few published papers that address the high Reynolds number cases.

For the square cylinder, the flow pattern in the wake region appears similar to the circular cylinder. However, the cause of flow separation in each of the two geometries is completely different. Because of the sharp leading edge at the corners, flow separation is governed by the geometry itself instead of the adverse pressure for circular cylinder, where the separation point moves back and forth on the circular cylinder surface. Because of the fixed separation point at the leading edges of the square cylinder, the aerodynamic characteristics are relatively insensitive to the Reynolds number compared to the circular cylinder. This type of geometric-dependent separation is used in some heat and mass transfer applications such as a flame holder in design of a combustor.[11]

Few computational studies have been conducted for flows past a circular cylinder at high Reynolds numbers. Breuer[12] used LES with second-order central difference for spatial derivatives and Runge–Kutta method for time marching with and without SGS models at a Reynolds number of 1.4×10^5. He showed that both the Smagorinsky and the dynamic SGS models provided results that agree fairly well with experimental data in velocity distributions and streamwise Reynolds stresses. However, the accuracy of the solution decreases with increase in distance from the cylinder due to the decrease in grid resolution. It is shown that changing Smagorinsky coefficient C_s can affect the solution. In Breuer's numerical experiment, $C_s = 0.1$ provided better results than $C_s = 0.065$. However, based on the results in terms of the streamwise and normal components of the velocity, it is difficult to identify which SGS model (Smagorinsky or dynamic) performs better. The cross-stream Reynolds stresses in his study are over predicted by both SGS models. The computations on the refined grid did not improve the results for either the cross-stream Reynolds stresses or shear stresses. This phenomenon also occurred in the low Reynolds number case, $Re = 3.9 \times 10^3$ (Ref. 13), but the reason is not clear. Therefore, additional and more extensive grid refinement investigations are required. The solution of LES without the SGS model, identified as cases A4 and B4, provided poor results. In contrast to the low Reynolds number case,[13] SGS models have more influence at higher Reynolds number. In general, however, the LES results were in reasonable agreement with experimental data. Travin et al.[14] used DES with a fifth-order upwind scheme and a structured grid. Because of numerical issues related to the upwind scheme in direct numerical simulation (DNS), LES or DES, they developed an algorithm that is centered in LES regions and upwind based in the RANS and irrotational regions. High Reynolds numbers of 1.4×10^5 and 3×10^6 were considered. Reynolds number of 1.4×10^5 was simulated at both subcritical laminar separation (LS) and supercritical turbulent separation (TS) cases. In reality, the $Re = 1.4 \times 10^5$ and $Re = 3 \times 10^6$ cases are at the high subcritical and supercritical range respectively. When the entire boundary layer is assumed to be turbulent, the flow properties of high subcritical flow will be similar to supercritical flow, thus, capturing flow properties at the supercritical range. Once the separation type is specified, the Reynolds number dependence should be weak. The results for $Re = 1.4 \times 10^5$ TS cases, both with fine and coarse grids, cases TS4 and TS5, with rotation/curvature (RC) term showed that the drag coefficient C_D, backpressure coefficient C_{pb}, and Strouhal number (Sr) compare better with the experimental results than without the RC term (cases TS1 and TS2). The drag coefficient is out of the experimental range for both cases TS1 and TS2. In the $Re = 1.4 \times 10^5$ LS cases, the solution provided lower C_D and the larger C_{pb} than experimental result, and the results on fine grid (case LS8) was better than the solution on coarse grid (case LS7). Squires et al.[15] using the DES code Cobalt simulated Reynolds number 8×10^5 on a structured grid, but only qualitative results were presented. Hansen and Forsythe[16] used an unstructured grid to simulate $Re = 1.4 \times 10^5$ (TS). The results in terms of Strouhal number Sr compared well with the experimental data, but the predicted drag coefficient C_D was lower than the experimental range. From the experimental results of Roshko,[9] the values of C_D, C_{pb}, and Strouhal number Sr approach constant values and are equal to 0.7, -0.85, and 0.27 respectively, when the Reynolds number is above 3.5×10^6. Achenbach[10] showed the experimental skin friction and C_p distributions from the high subcritical to the supercritical range. Cantwell and Coles[17] provided a well-documented experimental data for $Re = 1.4 \times 10^5$, which recorded both time-resolved and time-averaged data for future CFD tests.

Unlike the circular cylinder, which has received much attention in the past, the square/rectangular cylinder has received relatively less attention. Davis and Moore[18] presented numerical simulation by a one-dimensional QUICKEST scheme at low Reynolds numbers (1×10^2–2.8×10^3) for a two-dimensional rectangular cylinder. The Strouhal number compared well with experimental data for $Re < 1 \times 10^3$. Future work on grid refinement and fully three-dimensional simulation was suggested. Murakami et al.[19] focused on LES with several SGS models on three-dimensional square cylinder with both smooth and turbulent (6%) inflow conditions at $Re = 2.2 \times 10^4$. They found dynamic SGS model could improve the results remarkably in comparison with the standard Smagorinsky model. They also compared the two- and three-dimensional LES computations with the experimental results, which showed large discrepancies in the results of two-dimensional simulations. This is because the instantaneous flow structures are highly three dimensional for turbulence; therefore, three-dimensional simulation should be performed instead of two-dimensional simulation. Rodi et al.[20] provided two LES test cases and a collection of 10 groups with 16 sets of results for flows past a square cylinder at $Re = 2.2 \times 10^4$. The Strouhal number appeared to be less sensitive to the parameters of the simulation; however, the drag coefficient showed more deviation than the Strouhal number. The details on the various methods, such as the SGS, near-wall treatment, and grid points, may be found in Ref. 20. For the experimental data, Okajima[21] investigated the relationship between Strouhal number and Reynolds number for rectangular cylinder with different width and height ratio. Durao et al.[22] used a laser Doppler velocimeter to measure and quantify the turbulence and the periodic, nonturbulent motion of the square

cylinder wake flow in a water tunnel at $Re = 1.4 \times 10^4$. Lyn and Rodi[23] and Lyn et al.[24] provided detailed phase- (ensemble-) averaged and time-averaged velocities and turbulence intensities on the sidewalls of the cylinder for future turbulent model verification. Their experiment was performed in a closed water channel at $Re = 2.14 \times 10^4$ with freestream turbulence of 2%, and the corresponding Strouhal number was 0.134.

Because of the high computational cost for simulations at high Reynolds number by LES and the inefficiency of traditional wall models for separated flows, this study employed a DES approach to simulate flows past a circular cylinder at both subcritical and supercritical Reynolds numbers of 1.4×10^5 and 3.6×10^6. To simulate the supercritical flow properties, Travin et al.[14] used nonzero eddy viscosity at the inflow boundary condition for the high subcritical Reynolds number flow. In the present investigation, however, the supercritical case of $Re = 3.6 \times 10^6$ is simulated with the introduction of eddy viscosity by a trip function located on the surface of the cylinder. The square cylinder is simulated at a Reynolds number of 2.2×10^4, which includes two cases, LES without SGS (laminar option) and a DES/S–A model. The grid convergence investigation has been conducted at Reynolds number 1.4×10^4 by use of the DES/S–A model. Some cases were simulated on the coarse grid due to limitation of available computational resources. However, most of the solutions provided reasonable results. In addition, a comparison between the trip function and turbulent inflow was made for the supercritical flow.

II. Flow Solver

The code used in this research is Cobalt. Cobalt is a commercial CFD code, which is a cell-centered, finite volume, unstructured compressible flow solver. This code has been validated on several problems by Strang et al.[1] and Forsythe et al.[25]

Cobalt provides both RANS and DES approaches for turbulent simulations. In the DES approach, it contains both S–A and Menter's shear stress transport (M/SST) options. The current effort investigates turbulent flowfields with the DES/S–A formulation, and it is discussed in next section. More detailed information including the algorithm may be found in Refs. 1, 26, and 27.

III. DES

The original DES concept was proposed in 1997 by Spalart et al.[6] together with its formulation based on the S–A[7] one-equation turbulence model. This technique uses both LES and RANS formulations. It uses a single turbulence model, which functions as an SGS model in regions where the grid density is sufficiently fine for LES and as a RANS model in regions where it is not.[14] The fine grid means that Δ, the largest dimension of the local grid cell, is much smaller than the turbulence length scale l and still larger than Kolmogorov length scale. In LES regions, the larger scale eddies are resolved directly, and eddies smaller than Δ are left to the SGS model. In the near-wall region, the RANS model is used as a wall model to prevent decreasing of the filter width. Traditional LES wall models may have difficulties in the simulation of the separated flows and the grid refinement could exceed the computing power by several orders of magnitude. However, the RANS approach is known to be cost effective and has a certain credibility in boundary-layer calculations. When there are massive three-dimensional separations such as flow past a landing gear, or aircraft at high angle of attack, the accuracy of solution in this region is out of reach by the RANS approach. In contrast to the fairly standard eddies in the thin shear layer modeled by RANS, LES is an attractive choice for those geometry-specific eddies.

DES does not have an explicit filter operator similar to LES. The filter process is dependent on the grid spacing. In other words, the switching between RANS and LES depends on the grid design and can be controlled at preprocessing.

IV. DES/S–A Formulation

The S–A model solves a single differential equation for the working variable $\tilde{\nu}$, which is related to the eddy viscosity by $\nu_t = \tilde{\nu} f_{v1}$. The model includes a wall destruction term that reduces the turbulent viscosity in the viscous sublayer and log layer. The model contains a trip term that allows users to specify the transition location. With the trip term, the equation has the form

$$\frac{\mathrm{D}\tilde{\nu}}{\mathrm{D}t} = \frac{1}{\sigma}\left\{\nabla \cdot [(\nu + \tilde{\nu})\nabla\tilde{\nu}] + c_{b2}(\nabla\tilde{\nu})^2\right\} + c_{b1}\tilde{S}\tilde{\nu}(1 - f_{t2}) - \left[c_{w1} f_w - \frac{c_{b1}}{\kappa^2} f_{t2}\right]\left[\frac{\tilde{\nu}}{d_w}\right]^2 + f_{t1}(\Delta q)^2 \tag{1}$$

The turbulent kinematic viscosity is obtained from

$$\nu_t = \tilde{\nu} f_{v1}, \qquad f_{v1} = \chi^3 \big/ \left(\chi^3 + c_{v1}^3\right), \qquad \chi \equiv \tilde{\nu}/\nu \tag{2}$$

where S is the magnitude of the vorticity,

$$S = |\nabla \times V| \tag{3}$$

and the modified vorticity is

$$\tilde{S} \equiv S + \left(\tilde{\nu} \big/ \kappa^2 d_w^2\right) f_{v2}, \qquad f_{v2} = 1 - \chi/(1 + \chi f_{v1}) \tag{4}$$

where d_w is the distance to the nearest wall. The wall destruction function f_w is

$$f_w = g\left[\left(1 + c_{w3}^6\right) \big/ \left(g^6 + c_{w3}^6\right)\right]^{\frac{1}{6}} \tag{5}$$

where

$$g = r + c_{w2}(r^6 - r), \qquad r \equiv \tilde{\nu} \big/ \tilde{S}\kappa^2 d_w^2 \tag{6}$$

Large values of r should be truncated to a value of about 10. The function f_{t2} is given by

$$f_{t2} = c_{t3} \exp\left(-c_{t4}\chi^2\right) \tag{7}$$

The trip function is

$$f_{t1} = c_{t1} g_t \exp\left[-c_{t2}(\omega_t/\Delta q)^2\left(d_w^2 + g_t^2 d_t^2\right)\right] \tag{8}$$

where d_t is the distance from the field point to the trip that is located on the surface, ω_t is the wall vorticity at the trip, Δq is the difference between the velocities at the field point and trip, and $g_t = \min[1.0, \Delta q/\omega_t \Delta x]$, where Δx is the grid spacing along the wall at the trip.

The model coefficients are

$$\sigma = 2/3, \qquad c_{b1} = 0.1355, \qquad c_{b2} = 0.622$$

$$\kappa = 0.41, \qquad c_{w1} = c_{b1} \big/ \kappa^2 + (1 + c_{b2})/\sigma, \qquad c_{w2} = 0.3$$

$$c_{w3} = 2, \qquad c_{v1} = 7.1, \qquad c_{t1} = 1.0$$

$$c_{t2} = 2.0, \qquad c_{t3} = 1.1, \qquad c_{t4} = 2.0$$

When the trip term is turned off, the transport equation becomes

$$\frac{\mathrm{D}\tilde{\nu}}{\mathrm{D}t} = \frac{1}{\sigma}\left\{\nabla\cdot[(\nu+\tilde{\nu})\nabla\tilde{\nu}] + c_{b2}(\nabla\tilde{\nu})^2\right\} + c_{b1}\tilde{S}\tilde{\nu} - c_{w1} f_w \left[\frac{\tilde{\nu}}{d_w}\right]^2 \tag{9}$$

The presented wall destruction term is proportional to $(\tilde{\nu}/d_w)^2$, where d_w is the distance to the wall. When this term is balanced with the production term, the eddy viscosity becomes proportional to $\hat{S}d_w^2$, where $\hat{S}$ is the local strain rate. The Smagorinsky LES model varies its SGS turbulent viscosity with the local strain rate, and the grid spacing: $\nu_{\mathrm{SGS}} \propto \hat{S}\Delta^2$, where Δ generally depends on the local grid spacing. If d_w is replaced by Δ in the wall destruction term, and the production balance dissipation, the S–A model will act similarly to Smagorinsky model.

To exhibit both RANS and LES behavior, d_w in the S–A model is replaced by

$$\tilde{d} = \min(d_w, C_{\mathrm{DES}}\Delta) \tag{10}$$

where Δ is based on the largest dimension of the grid cell,

$$\Delta = \max(\Delta x, \Delta y, \Delta z) \tag{11}$$

When $d_w < C_{\mathrm{DES}}\Delta$, the RANS formulation is implemented, and when $d_w > C_{\mathrm{DES}}\Delta$ the model acts in the LES mode. In the attached boundary layer, due to the significant grid anisotropy ($\Delta x \approx \Delta z \gg \Delta y$), $\tilde{d} = d_w$, the model is the standard S–A RANS model. However, the LES formulation can be implemented in that region if the grid is refined sufficiently such that turbulence can be resolved in all three directions. Once the cell is sufficiently far from the walls ($d_w > C_{\mathrm{DES}}\Delta$), such as in the separation region, the length scale of the model becomes grid dependent and the model performs as an SGS version of the S–A model. The empirical constant C_{DES} was calibrated to 0.65 and is not very critical.[28]

V. Grid Generation

All of the grids were generated by GAMBIT (data available online at http://www.fluent.com/software/gambit/index.htm) and subsequently converted to Cobalt suitable format by an in-house code. Figures 1 shows the surface grids of the cylinders. Flow is in the positive x direction. Figure 2 shows the entire domain mesh, and Fig. 3 show the mesh in the near-wall regions. The mesh on the

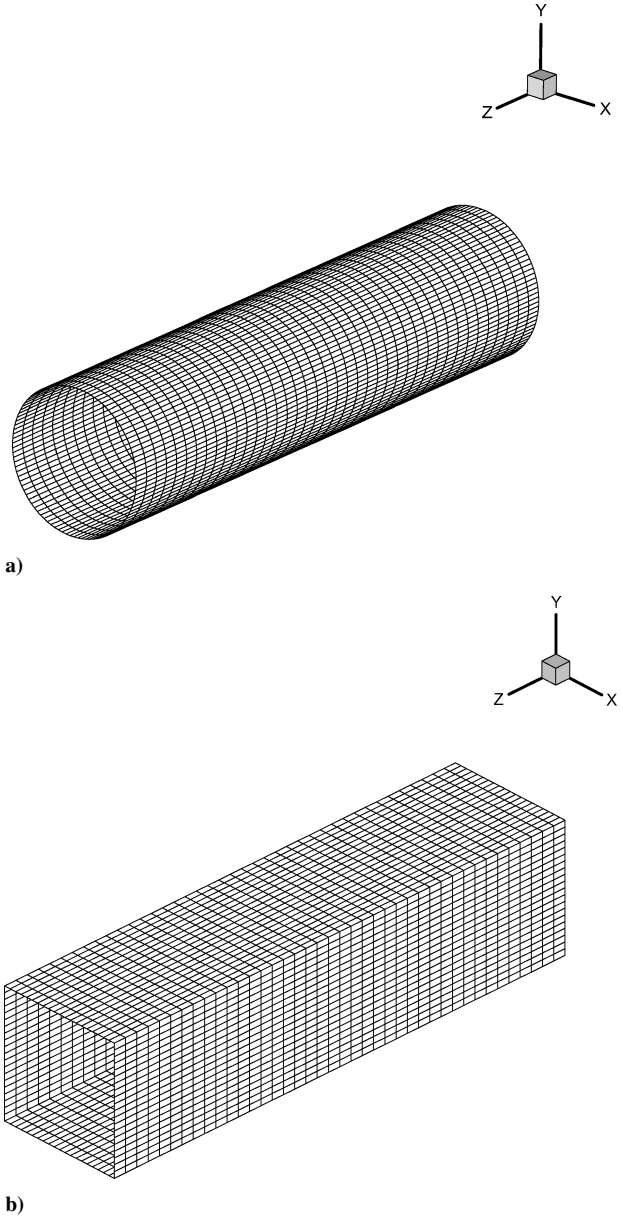

Fig. 1 Surface grid: a) circular cylinder and b) square cylinder.

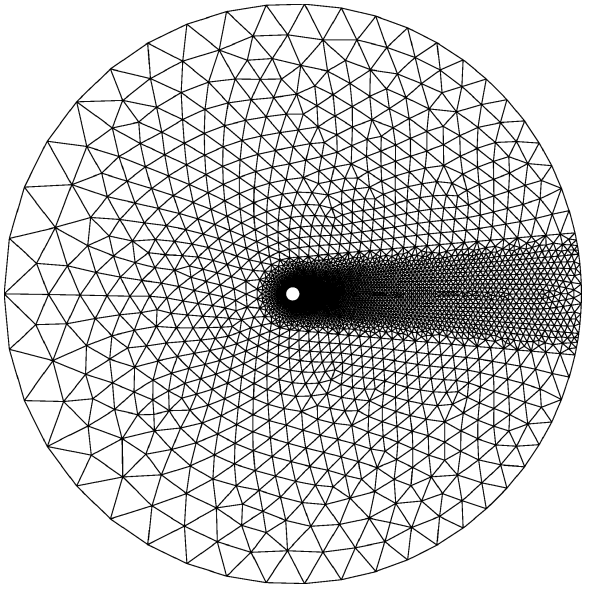

Fig. 2 Grid in crossflow plane.

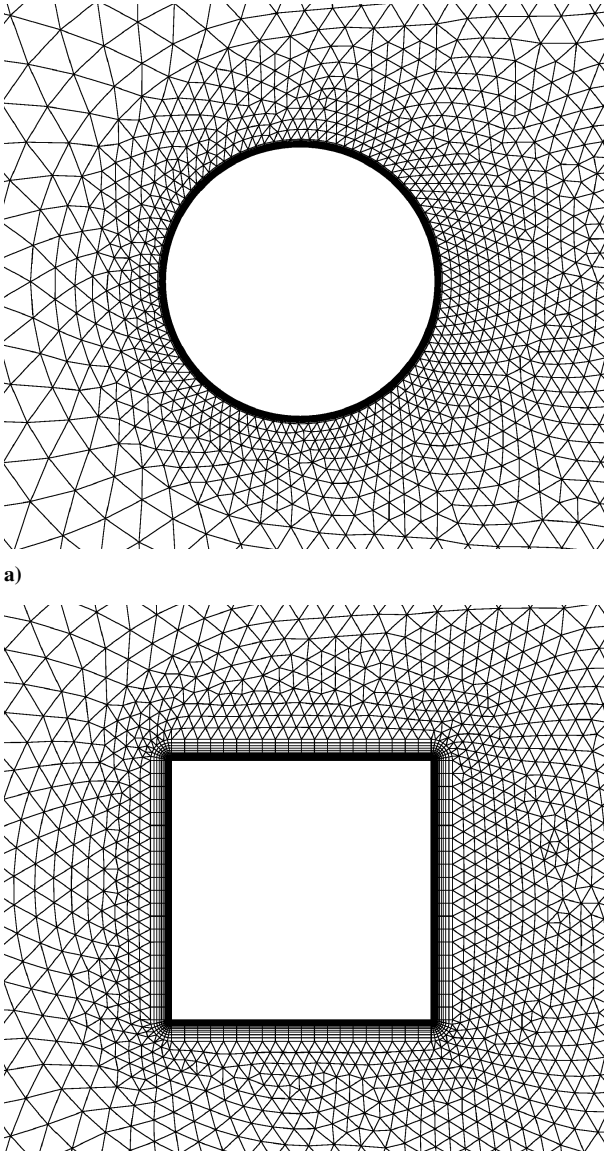

Fig. 3 Grid in near wall region: a) circular cylinder and b) square cylinder.

Table 1 Summary of test cases

Run	Re	Grid	Span	L_r/D	C_D	C_{pb}	Sr	θ_{sep}, deg
A1-LS	1.4×10^5	428,677	$2D$	0.608	0.98	−0.913	0.196	84
A2-LS	1.4×10^5	471,208	$1D$	0.608	0.943	−0.884	0.22	84
Breuer (A2)[12]	1.4×10^5	$165 \times 165 \times 64$	$2D$	0.416	1.218	−1.411	0.217	95.16
Travin et al. (LS8)[14]	1.4×10^5	$150 \times 109 \times 42$	$2D$	1.1	1.08	−1.04	0.21	77
Cantwell and Coles (experiment)[17]	1.4×10^5	∼	$30D$	0.44	1.237	−1.21	∼0.2	77
B1-TS	1.4×10^5	428,677	$2D$	0.6	0.62	−0.834	0.294	105
B2-TS	1.4×10^5	471,208	$1D$	0.6	0.704	−0.914	0.287	104.5
B3-TS (180)	1.4×10^5	706,012	$2D$	0.81	0.65	−0.75	0.305	100
B4-TS (240)	1.4×10^5	960,454	$2D$	0.64	0.67	−0.85	0.287	101
Hansen and Forsythe[16]	1.4×10^5	>1,434,605	$4D$	∼	0.59	−0.72	0.29	∼
Travin et al. (TS1)[14]	1.4×10^5	$118 \times 105 \times 30$	$2D$	1.1	0.57	−0.65	0.3	99
Roshko (experiment)[9]	$>3.5 \times 10^6$	∼	∼	∼	0.62 ∼ 0.74	−0.85	0.27	∼
C1-TS	3.6×10^6	539,152	$2D$	0.35	0.576	−0.796	0.305	118
C2-Trip 65 deg	3.6×10^6	539,152	$2D$	0.32	0.535	−0.748	0.311	119
Achenbach (experiment)[10]	3.6×10^6	∼	$10D/3$	∼	0.76	−0.85	0.27	115

[a]Structured grid sizes are in terms of number of nodes in the radial, azimuthal, and spanwise directions.

cylinder surface is set to 100 or 110 nodes in the azimuthal direction, except for case B3 (180 nodes) and B4 (240 nodes). Spanwise distance is set to two diameters with 20 nodes per diameter. The periodic boundary conditions were used in both positive and negative z planes. Modified Riemann invarients are used for the far-field boundaries. The total cell numbers for each case are summarized in Table 1. The far-field boundaries are placed 20 diameters away from the cylinder surface. For the $Re = 3.6 \times 10^6$ case, the trip location is specified from ±65 to ±85 deg measured from the stagnation point, as reported by Achenbach.[10] The average y^+ are 0.065 and 0.4 for Reynolds numbers of 1.4×10^5 and 3.6×10^6, respectively. The grid for the square cylinder was generated in a similar fashion as the grid for the circular cylinder grid. Because of the 90-deg corner of the square cylinder, the boundary-layer mesh there is more challenging to design than the circular section. The grid is clustered near the corners. The total cell numbers are 466,424 and the average y^+ at Reynolds number $Re = 2.2 \times 10^4$ is 0.065.

VI. Simulations and Results

Circular Cylinder at $Re = 1.4 \times 10^5$

A circular cylinder in a crossflow at Reynolds number $Re = 1.4 \times 10^5$ is simulated at Mach = 0.1 for both the subcritical and the supercritical regimes. The LES without SGS (laminar option in Cobalt) was used in the subcritical simulation, and the fully turbulent flow was simulated with the DES/S–A approach for the supercritical region. All computations were performed at the High Performance Computing Center at Wichita State University, which operates a Silicon Graphics Origin 2000 machine and two cluster machines. The Origin 2000 machine contains 24 processors (where 16 operate at 300 MHz and 8 at 250 MHz), with 10 GBytes RAM. Each cluster machine has 32 processors and use 2.66-GHz Xeon processors. Because of the imposed limitations, only 4–12 processors are used for each parallel execution. The CPU time for the 428,677-cell grid with 8 processors is about 2.2×10^{-4} s per iteration per cell on the Origin 2000 machine and 5.3×10^{-5} s on the cluster machine.

The nondimensional time step is set to 0.01 (based on the freestream velocity and cylinder diameter), providing more than 300 data points for each shedding cycle. Three Newton subiterations were used to reduce linearization errors of the implicit scheme. A stationary solution is typically established at about 40–100 nondimensional time units. Therefore, the time-averaged values begin from 100 nondimensional time units. In all cases, the averages are computed at least 200 nondimensional time units, corresponding to about 40 and 54 shedding cycles for the LS and TS cases, respectively.

Figure 4 shows the relationship between the Strouhal number and the time step for the B1 case. It shows that the Strouhal number is sensitive to time step. The Strouhal number increases with decreasing the time step until it approaches a constant value of about 0.294 when $\Delta t < 0.02$. This provides some assurance for the selection of 0.01 as the suitable time step.

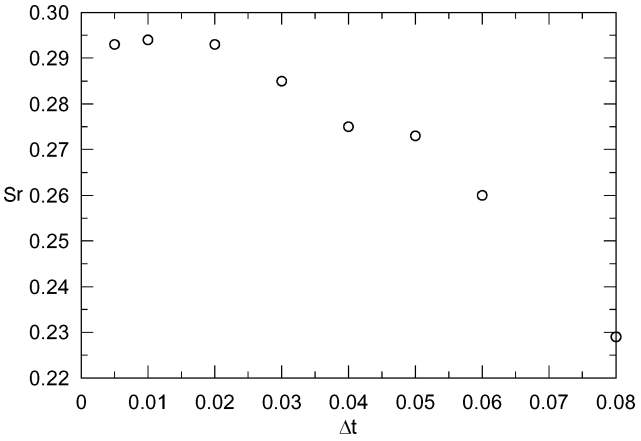

Fig. 4 Strouhal number vs time step.

Table 1 shows the relevant cases investigated in the current study and from other investigators, including both numerical and experimental results. The drag coefficient C_D is computed from the oscillation force in the x direction. The base pressure coefficient C_{pb} is defined as the pressure coefficient on the centerline of the leeward side of the cylinder (trailing edge). The L_r/D is the nondimensional length of the recirculation zone in the wake region. These parameters are computed by averaging in both time and space (spanwise). The Strouhal number is computed from $Sr = fD/U_\infty$, where f is the shedding frequency taken from the lift curve, D is the diameter, and U_∞ is the freestream velocity. The A1-LS and A2-LS cases are simulated by LES without SGS, which resolves the turbulent properties directly. Cases B1–B4 used the turbulent DES/S–A approach to mimic the turbulent boundary layer in the supercritical region. Case C1-TS is performed similar to case B, and the C2-trip 65 deg introduces the trip function specified from ±65 deg measured from the stagnation point.

For the subcritical regime, both the A1-LS and A2-LS cases compare well with the experimental results except for the drag coefficient, which is slightly underpredicted. For the supercritical regime, the C_D, C_{pb}, and Strouhal number Sr for all B cases are within the experimental range and compare better to the experimental results than most other published numerical results. The spanwise resolution in the current study does not show a significant effect on these parameters, nor on pressure and velocity distributions.

Figure 5 shows the oscillations in lift and drag coefficients with nondimensional time for A1-LS case. The Strouhal number $Sr = 0.196$, which compares well with the experimental result of 0.2. The average drag coefficient is 0.98, which is about 20% lower than the experimental result.

Figure 6 shows a comparison of the time-averaged pressure coefficient for the $Re = 1.4 \times 10^5$ LS case. The data also include spanwise

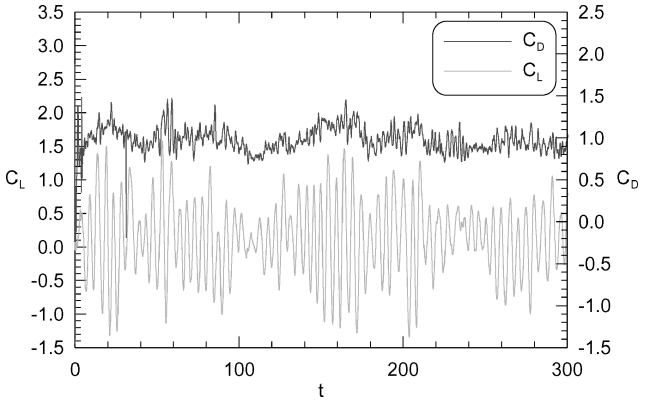

Fig. 5 Time-dependent force coefficients for A1-LS case.

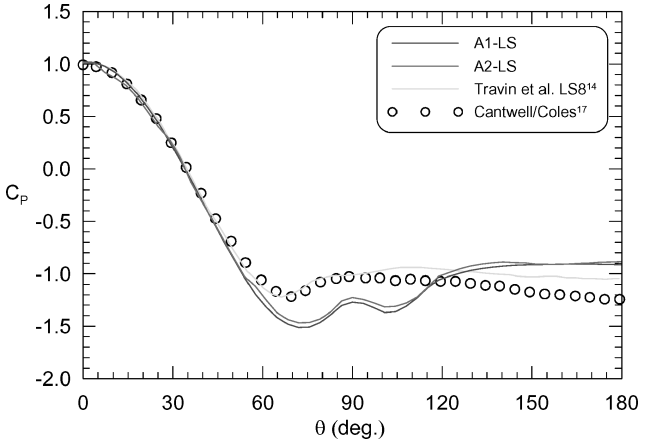

Fig. 6 Pressure coefficients on cylinder surface for $Re = 1.4 \times 10^5$ LS cases.

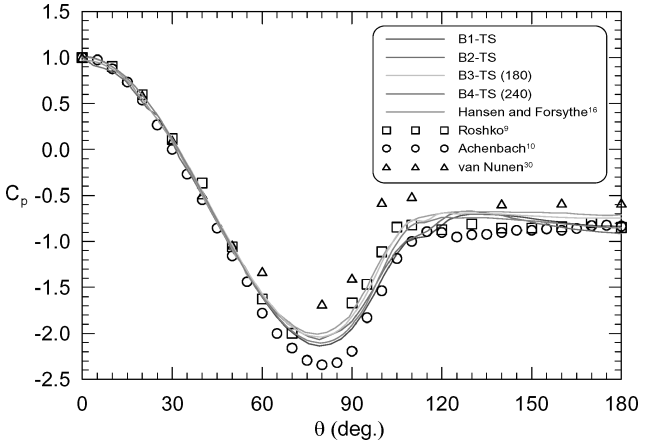

Fig. 7 Pressure coefficients on cylinder surface for $Re = 1.4 \times 10^5$ TS cases.

averaging. The angle θ is measured from the leading-edge stagnation point, which corresponds to 0 deg. Other numerical and experimental results are taken from Refs. 14 and 17 and correspond to the same Reynolds number. Both case A1-LS and A2-LS provide almost identical results. In the results of Travin et al.,[14] the medium grid case, LS8, shows the backpressure coefficient is about 8% higher, whereas their coarse grid case LS7 is about 36% higher compared to the experimental results. The results (cases A1 and A2) of current investigation yield backpressures that fall between the LS7 and LS8 cases. The dips occurring around $\theta = 100$ deg can be attributed to the large grid point spacing in the cylinder circumferential direction and can be eliminated by increasing grid points, as shown in Fig. 7.

Figure 7 shows a comparison of the time-averaged pressure coefficient for the $Re = 1.4 \times 10^5$ TS case. DES results by Hansen and Forsythe[16] are also presented for comparison. Experimental data taken at supercritical Reynolds numbers of 8.4×10^6, 3.6×10^6, and 7.6×10^6, which correspond to data of Roshko,[9] Achenbach,[10] and van Nunen,[29] respectively, are included in Fig. 7. The present simulations show the results for a different circumferential resolution. Both cases B1 and B2 have 100 points, case B3 has 180 points, and case B4 has 240 points in the circumferential direction. The spanwise grid distribution has a small effect on the C_p distribution. The difference with the results of Hansen and Forsythe[16] can be attributed to different cell geometries in the near-wall region and the total number of grid points used.

Figures 8–11 show comparisons of the time-averaged velocity distributions for the $Re = 1.4 \times 10^5$ LS case at different streamwise

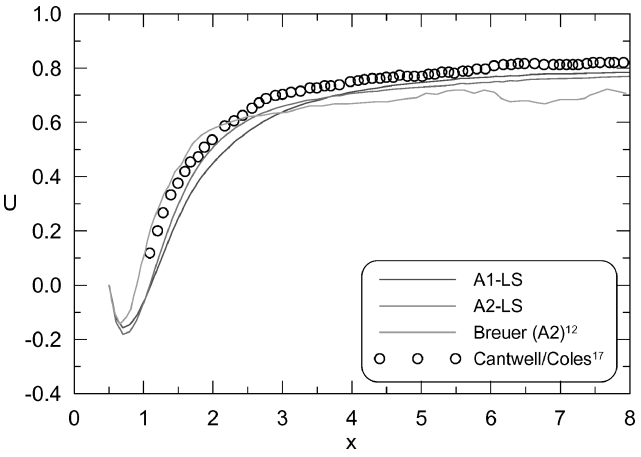

Fig. 8 Time-averaged streamwise velocity at axis $y = 0$.

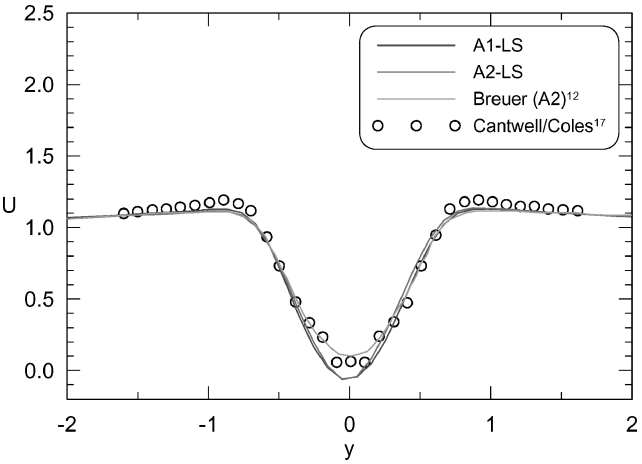

Fig. 9 Time-averaged streamwise velocity at $x = 1$.

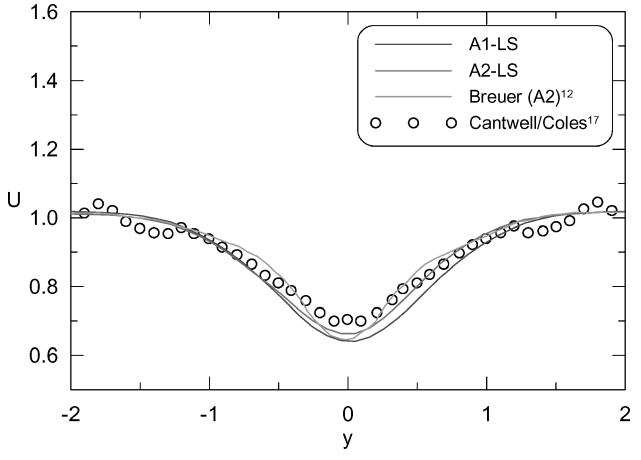

Fig. 10 Time-averaged streamwise velocity at $x = 3$.

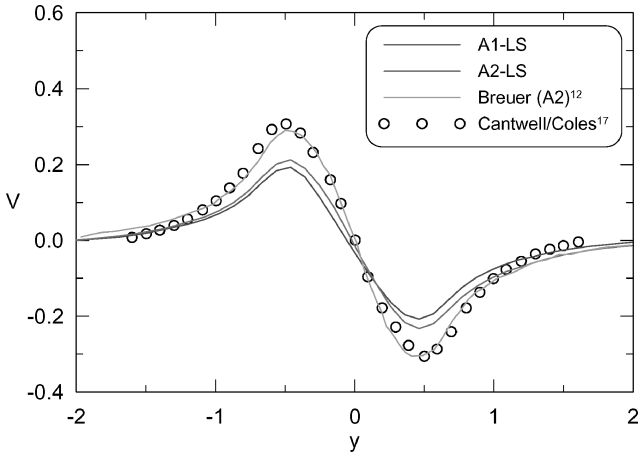

Fig. 11 Time-averaged normal velocity at $x = 1$.

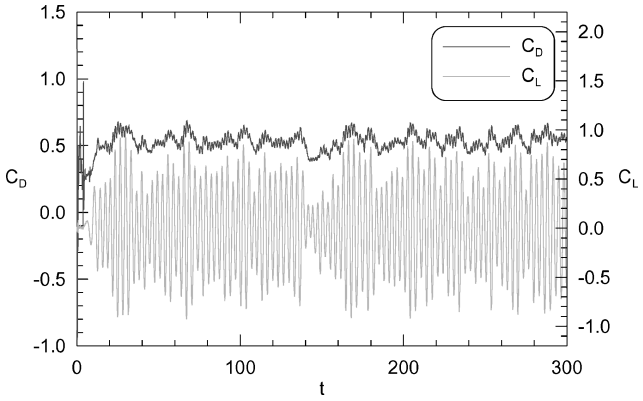

Fig. 12 Time-dependent force coefficients for C2-trip 65-deg case.

locations. Breuer's[12] A2 case was performed with LES and the Smagorinsky model and without using any wall model. The experimental data were taken from Ref. 12, which was performed by Cantwell and Coles.[17] The streamwise velocity (Fig. 8) of both current cases slightly overpredicts the recirculation length behind the cylinder. However, beyond $x > 3$, the velocity recovery of the current cases appear better than Breuer's result. This may be attributed to his grid resolution becoming coarser in the far wake region.

All of the streamwise velocities at $x = 1$ and 3 (Figs. 9 and 10) compare well with the experimental results. However, the normal component of velocity (Fig. 11) for the current cases slightly underpredicts the experimental results. This is primarily due to the grid resolution.

Circular Cylinder at $Re = 3.6 \times 10^6$

The grid used for this simulation is similar to the $Re = 1.4 \times 10^5$ case and has 539,152 cells. Two cases are investigated at Reynolds number $Re = 3.6 \times 10^6$. The first case employs fully turbulent incoming flow, causing the boundary layer to be turbulent, which is similar to the $Re = 1.4 \times 10^5$ TS case. The second case employs laminar incoming flow with the trip function located from ± 65 to ± 85 deg measured from the stagnation point. This transition location is reported by Achenbach.[10] The flow Mach number is 0.1. Time averages are taken after 100 nondimensional time units. Table 1 shows a summary of the results of current study and experimental data. Both cases have underpredicted the drag by about 25%. The trip case does not show any improvement compared with the fully turbulent case, even though its flowfield is closer to the experimental condition rather than the C1-TS case. This is in contrast to the original expectation. Our other numerical experiments also show that aerodynamic parameters are insensitive to moving the trip location forward to ± 45 deg.

Figure 12 shows the time-dependent lift and the drag coefficients for trip case. The Strouhal number is 0.311, higher than the experimental value of 0.27. The average drag coefficient is much lower compared to the $Re = 1.4 \times 10^5$ TS cases.

Table 2 Aerodynamic parameters for square cylinder at $Re = 2.2 \times 10^4$

Cases	Grid	C_D	Sr	C_{pb}	L_r/D
D1-TS	466,424	2.3	0.14	−1.53	0.6
D2-LS	466,424	2.18	0.134	−1.5	0.81
UKAHY2[20]	$146 \times 146 \times 20$	2.3	0.13	∼	0.96
TAMU2[20]	$165 \times 113 \times 17$	2.77	0.14	∼	0.44
Experiment[23,24]	∼	1.9 ∼ 2.2	0.132	∼	0.88

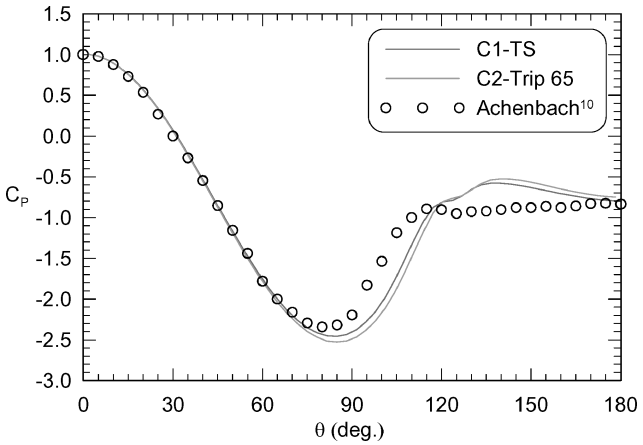

Fig. 13 Pressure coefficients on cylinder surface for $Re = 3.6 \times 10^6$ cases.

Figure 13 shows a comparison of the time-averaged pressure coefficient on the cylinder surface with the experimental data of Achenbach[10] at the same Reynolds number. The two cases compare well with each other and have little sensitivity to the trip function. Some minor deviation occurs beyond $\theta > 90$ deg. However, the backpressure compares very well with the experimental results.

Square Cylinder at $Re = 2.2 \times 10^4$

A square cylinder at Reynolds number $Re = 2.2 \times 10^4$ is simulated at Mach $= 0.1$ with both laminar and turbulent flowfields. DES/S–A and LES without SGS were used for this simulation. The CPU time for the 466,424 cells grid with 8 processors is about 5.85×10^{-5} s per iteration per cell on the cluster machine. The nondimensional time (based on freestream velocity and side length) of 0.01 was used for all simulations based on the success of the circular cylinder cases. The time average starts from 100 nondimensional time units, and all averaged values are computed at least 200 nondimensional time units, corresponding to about 24 shedding cycles.

Table 2 shows a summary of the aerodynamic parameters for the current investigation and other numerical and experimental results. LS and TS designate the LES without SGS and DES/S–A simulations, respectively. The experimental data are from Lyn and Rodi[23] and Lyn et al.,[24] for $Re = 2.2 \times 10^4$. The other numerical results, UKAHY2 and TAMU2, are from Rodi et al.,[20] for experiments performed by other research groups. Both UKAHY2 and TAMU2 cases use LES with the Smagorinsky model and dynamic SGS model, respectively, and use wall functions for near-wall treatment with zero inflow turbulence. In the current study, the D1 case predicts slightly higher Strouhal number compared to the experiment result. However, accurate prediction of the Strouhal number is not necessarily an indication of a quality simulation because it is not very sensitive to the parameters of the simulation.[20] The time-averaged drag coefficients are slightly higher than the experimental result for all of the numerical data except the D2 case, and the recirculation lengths also have some deviations with respect to the experimental results. In fact, in Ref. 20, it is shown that both the drag coefficient and recirculation length are highly sensitive to the near-wall treatment

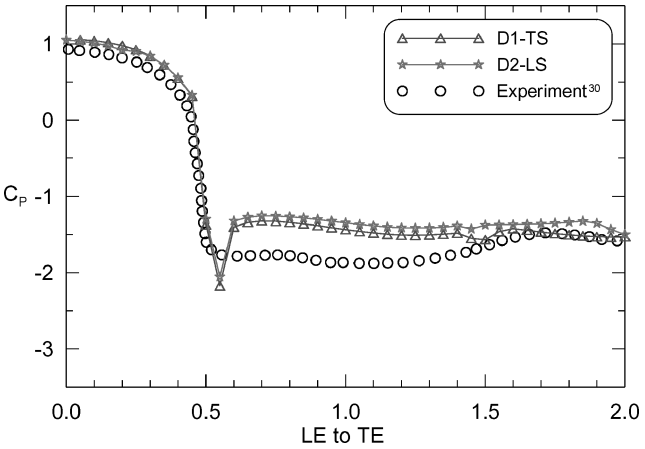

Fig. 14 Pressure coefficients on cylinder surface at $Re = 2.2 \times 10^4$.

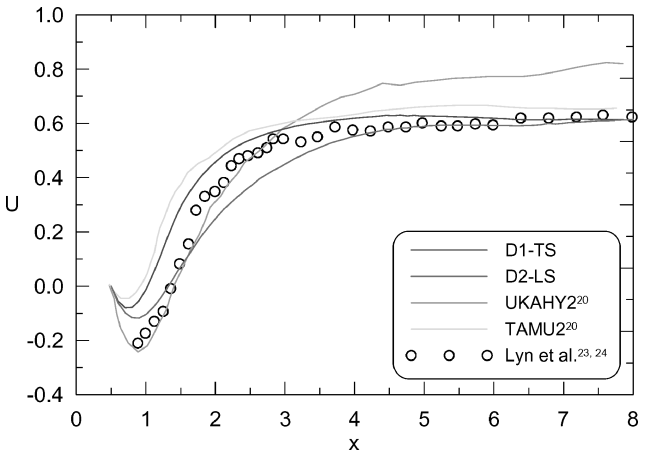

Fig. 15 Time-averaged streamwise velocity along $y = 0$.

and the resolution near the surface. Those cases that use the no-slip boundary condition have results even worse than those using wall functions.

Figure 14 shows a comparison of the time-averaged pressure distributions around the upper surface of the cylinder with the experimental data.[30] The numerical data were averaged in the spanwise direction and taken from the stagnation point at $y = 0$ and around the wall to the trailing edge at $y = 0$. The symbols on both numerical curves represent the grid point locations on the cylinder wall. Both the D1 and D2 cases predict slightly higher stagnation pressure, $C_p \sim 1.05$. Flow separations occur at the upper and lower front corner. The current simulations predict lower C_p compared the experimental data (about 20%) around the corners. The back pressure for both cases compares well with the experiment results.

Figure 15 compares the time-averaged streamwise velocity along the symmetry line along $y = 0$. The D1 case predicts smaller recirculation length. However, both velocity distributions are better than other numerical results beyond $x > 2.5$, especially when compared to UKAHY2, which shows large deviations. The TAMU2 case shows even smaller recirculation length and larger minimum velocity than the current cases. For $x < 2$, the differences in results can be attributed to the near-wall treatment and the grid resolution near cylinder. For $x > 2$ (wake region), the result is more dependent on the grid resolution.

VII. Conclusions

Flow past cylinders with circular and square cross sections were simulated at both subcritical and supercritical regimes. Because of the limitations of the computational resources, most of the current studies were performed on relatively coarse grids. However, the results of all cases compare well with the experiment data and other numerical results, which had employed finer grid than current study.

At subcritical Reynolds number $Re = 1.4 \times 10^5$, different span resolutions were investigated for the circular cylinder. In the current study, this parameter did not affect the solution significantly. The computed aerodynamic parameters compared well with the experimental and other numerical results. The laminar streamwise velocities also compared well with the experimental data; however, the normal velocity showed some deviation.

For the supercritical Reynolds number, the results of $Re = 1.4 \times 10^5$ simulation with fully turbulent boundary-layer assumption fall within the experiment range and are better than most other numerical results. Instead of assuming a fully turbulent boundary layer, the $Re = 3.6 \times 10^6$ cases investigated the effect of the transition. The results showed that the trip function has little effect on the aerodynamic parameters, whether it is used or not. From our numerical experiments, the location of the trip function also shows little effect on the aerodynamic parameters such as C_D, C_{pb}, and Strouhal number Sr. The aerodynamic parameters for $Re = 3.6 \times 10^6$ show some deviation compared to the experimental data. This situation may be because this test Reynolds number is too close to the critical range and/or the grid resolution. In the critical range, the experimental data are highly scattered, which makes numerical comparison more difficult.

The square cylinder cases were simulated at Reynolds number $Re = 2.2 \times 10^4$ with both LES without SGS and with the DES/S–A approach. The DES/S–A case predicts slightly higher Strouhal number and lower recirculation length than the experimental results. However, the streamwise velocity and pressure coefficient distributions for both current cases compare well with the experimental data.

Acknowledgments

The authors acknowledge the support of National Science Foundation under Grant EIA-0216178 and Grant EPS-0236913, matching support from the State of Kansas and the Wichita State University High Performance Computing Center.

References

[1]Strang, W. Z., Tomaro, R. F., and Grismer, M. J., "The Defining Methods of Cobalt$_{60}$: A Parallel, Implicit, Unstructured Euler/Navier–Stokes Flow Solver," AIAA Paper 99-0786, Jan. 1999.

[2]Forsythe, J. R., Squires, K. D., Wurtzler, K. E., and Spalart, P. R., "Detached-Eddy Simulation of Fighter Aircraft at High Alpha," AIAA Paper 2002-0591, Jan. 2002.

[3]Mitchell, A., Morton, S., and Forsythe, J. R., "Analysis of Delta Wing Vortical Substructures Using Detached-Eddy Simulations," AIAA Paper 2002-2968, Jan. 2002.

[4]Morton, S. A., Forsythe, J. R., Squires, K. D., and Wurtzler, K. E., "Assessment of Unstructured Grids for Detached-Eddy Simulation of High Reynolds Number Separated Flows," *Proceedings of the Eight International Conference on Numerical Grid Generation in Computational Field Simulations*, Honolulu, June 2002.

[5]Baggett, J. S., "Some Modeling Requirements for Wall Models in Large Eddy Simulation," *Annual Research Briefs 1997*, Center for Turbulence Research, NASA Ames/Stanford Univ., Stanford, CA, pp. 123–134.

[6]Spalart, P. R., Jou, W.-H., Strelets, M., and Allmaras, S. R., "Comments on the Feasibility of LES for Wings, and on a Hybrid RANS/LES Approach," *Advance in DNS/LES, 1st AFOSR International Conference on DNS/LES*, Greyden Press, Columbus, OH, 1997.

[7]Spalart, P. R., and Allmaras, S. R., "A One-Equation Turbulence Model for Aerodynamic Flows," AIAA Paper 92-0439, Jan. 1992.

[8]Strelets, M., "Detached Eddy Simulation of Massively Separated Flows," AIAA Paper 2001-0879, Jan. 2001.

[9]Roshko, A., "Experiments on the Flow Past a Circular Cylinder at Very High Reynolds Number," *Journal of Fluid Mechanics*, Vol. 10, No. 3, 1961, pp. 345–356.

[10]Achenbach, E., "Distribution of Local Pressure and Skin Friction Around a Circular Cylinder in the Cross-Flow up to $Re = 5 \times 10^6$," *Journal of Fluid Mechanics*, Vol. 34, No. 4, 1968, pp. 652–639.

[11]Younger, G. G., Gabriel, D. S., and Mickelsen, W. R., "Experimental Study of Isothermal Wake–Flow Characteristics of Various Flame-Holder Shapes," NACA RM E51K07, Jan. 1952.

[12]Breuer, M., "A Challenging Test Case for Large Eddy Simulation: High Reynolds Number Circular Cylinder Flow," *International Journal of Heat and Fluid Flow*, Vol. 21, No. 5, 2000, pp. 648–654.

[13]Breuer, M., "Large Eddy Simulation of the Subcritical Flow Past a Circular Cylinder: Numerical and Modeling Aspects," *International Journal of Numerical Methods in Fluids*, Vol. 28, No. 9, 1998, pp. 1281–1302.

[14]Travin, A., Shur, M., Strelets, M., and Spalart, P., "Detached-Eddy Simulations Past a Circular Cylinder," *Flow, Turbulence and Combustion*, Vol. 63, Nos. 1–4, 1999, pp. 293–313.

[15]Squires, K. D., Forsythe, J. R., Morton, S. A., Strang, W. Z., Wurtzler, K. E., Tomaro, R. F., Grismer, M. J., and Spalart, P. R., "Progress on Detached-Eddy Simulation of Massively Separated Flow," AIAA Paper 2002-1021, Jan. 2002.

[16]Hansen, R. P., and Forsythe, J. R., "Large and Detached Eddy Simulation of a Circular Cylinder Using Unstructured Grids," AIAA Paper 2003-0775, Jan. 2003.

[17]Cantwell, B., and Coles, D., "An Experimental Study of Entrainment and Transport in the Turbulent Near Wake of a Circular Cylinder," *Journal of Fluid Mechanics*, Vol. 136, 1983, pp. 321–374.

[18]Davis, R. W., and Moore, E. F., "A Numerical Study of Vortex Shedding from Rectangles," *Journal of Fluid Mechanics*, Vol. 116, 1982, pp. 475–506.

[19]Murakami, S., Iizuka, S., and Ooka, R., "CFD Analysis of Turbulent Flow past Square Cylinder Using Dynamic LES," *Journal of Fluids and Structures*, Vol. 13, No. 78, 1999, pp. 1097–1112.

[20]Rodi, W., Ferziger, J. H., Breuer, M., and Pourquie, M., "Status of Large Eddy Simulation: Results of a Workshop," *Journal of Fluids Engineering*, Vol. 119, No. 2, 1997, pp. 248–262.

[21]Okajima, A., "Strouhal Numbers of Rectangular Cylinders," *Journal of Fluid Mechanics*, Vol. 123, 1982, pp. 379–398.

[22]Durao, D. F. G., Heitor, M. V., and Pereira, J. C. F., "Measurements of Turbulent and Periodic Flows Around a Square Cross-Section Cylinder," *Experiments in Fluids*, Vol. 6, No. 5, 1988, pp. 298–304.

[23]Lyn, D. A., and Rodi, W., "A Flapping Shear Layer Formed by Flow Separation from the Forward Corner of a Square Cylinder," *Journal of Fluid Mechanics*, Vol. 267, 1994, pp. 353–376.

[24]Lyn, D. A., Einav, S., Rodi, W., and Park, J.-H., "A Laser-Doppler Velocimetry Study of Ensemble-Averaged Characteristics of Turbulent Near Wake of a Square Cylinder," *Journal of Fluid Mechanics*, Vol. 304, 1995, pp. 285–319.

[25]Forsythe, J. R., Strang, W., and Hoffmann, K. A., "Validation of Several Reynolds-Averaged Turbulence Models in a 3D Unstructured Grid Code," AIAA Paper 2000-2552, June 2000.

[26]Tomaro, R. F., Strang, W. Z., and Sankar, L. N., "An Implicit Algorithm for Solving Time Dependent Flows on Unstructured Grids," AIAA 97-0333, Jan. 1997.

[27]Cobalt User's Manual, Cobalt Ver. 2.0, Cobalt Solution, LLC, Springfield, OH.

[28]Shur, M. L., Spalart, P. R., Strelets, M. K., and Travin, A., "Detached-Eddy Simulation of an Airfoil at High Angle of Attack," *4th International Symposium on Engineering Turbulence Modelling and Measurements*, edited by W. Rodi and D. Laurence, Elsevier, Amsterdam, 1999, pp. 669–678.

[29]van Nunen, J. W. G., "Pressure and Forces on a Circular Cylinder in a Cross Flow at High Reynolds Number," *Flow Induced Structural Vibrations*, edited by E. Naudasher, Springer–Verlag, Berlin, 1974, pp. 748–754.

[30]Bearman, P. W., and Obasaju, E. D., "An Experimental Study of Pressure Fluctuations on Fixed and Oscillating Square-Section Cylinders," *Journal of Fluid Mechanics*, Vol. 119, 1982, pp. 297–321.